Reprinted from

Seventh International Symposium

Machine Processing of

Remotely Sensed Data

with special emphasis on

Range, Forest and Wetlands Assessment

June 23 - 26, 1981

Proceedings

Purdue University
The Laboratory for Applications of Remote Sensing
West Lafayette, Indiana 47907 USA

LANDSAT D THEMATIC MAPPER IMAGE RESAMPLING FOR SCAN GEOMETRY CORRECTION

ARUN PRAKASH, ERIC P. BEYER

General Electric Company
Philadelphia, Pennsylvania

I. ABSTRACT

The Landsat D Project will use, for the first time, a new sensor called the Thematic Mapper. This sensor is a mechanically scanned radiometer with seven spectral bands, which images the earth from space with a thirty meter spatial resolution. It will provide enhanced remote sensing capabilities relative to earlier Landsats, through improved spatial, spectral and radiometric resolution, global coverage and more rapid processing of data for users.

To meet high throughput rates and stringent accuacy requirements, new hardware architecture and novel algorithms for data processing are used. Image data is received on the ground at a 84.9 megabit/sec rate and is processed to generate output images at 750,000 pixels per second or faster. Image processing on the ground proceeds in three steps. First, the sample intensities are radiometrically corrected. Next, the input sample positions are determined on a map grid. Finally, the output image is generated. The last step is called resampling.

The resampling procedure is analyzed in this paper, with particular emphasis on the effect that the sampling geometry has on the output image. Scan gaps and spacecraft jitter effects on the output image are studied by performing a simulation of the sampling and the resampling processes. The images produced under different scan geometries are displayed for visual assessment. Another means of comparing images to detect geometric distortion and radiometric error is developed. This is the difference image histogram, and it can be used to characterize the resampling errors. The results show that the resampling algorithm works excellently under all conditions. Distortion is visible only under extremely large scan gap conditions which rarely occur.

II. SYSTEM

A. LANDSAT D SYSTEM OVERVIEW[2]

Landsat D is an earth resources observational system which will offer significant improvements over the previous Landsat 1, 2 or 3 systems. General Electric Company is the Landsat D Mission System Contractor and is responsible for system performance, spacecraft (flight segment) integration and test and development of the ground processing system (ground segment) for NASA Goddard Space Flight Center. The flight segment and Multispectral Scanner (MSS) ground processing will be operational in 1982. The Thematic Mapper (TM) processing system will begin operation in 1983 and progress to full throughput capability in 1984.

The Landsat D flight segment is shown in Figure 1. It includes an improved attitude control in both pointing accuracy and stability; precision attitude determination systems which measure over a bandwidth of 0 to 125 Hz; extensive communication capability including both direct readout channels and communication through the NASA Tracking and Data Relay Satellite System (TDRSS); a Multispectral Scanner (MSS) imaging instrument which is similar to that of the previous Landsat systems; and a Thematic Mapper (TM) imaging instrument which will provide significant improvements in spectral resolution, spectral coverage and spatial resolution over the MSS.

In concept, the TM design is similar to that of the MSS. The TM uses an oscillating scan mirror to sweep detectors across the track of the spacecraft motion. The TM images in both the forward and reverse scan directions while the MSS scans in one direction. The TM bi-directional scanning affords greater scan efficiency, 80% for TM as compared to 45% for MSS, but additional processing complexity is required to handle geometric discontinuity between scans. Other

* This work was supported by NASA Contract No. NAS 5-25300.

significant differences between the TM and MSS are listed below:

	TM	MSS
Ground Sample Distance (meters)	30 x 30	82 x 56
Scan Frequency (Hz)	7.0	13.62
Number of Spectral Bands	7	4
Maximum Focal Plane Distance Between Bands (samples)	183	6
Detectors/Band	16	6

The Landsat D ground segment consists of a Mission Management which provides for mission planning and production control; a Control and Simulation Facility which provides flight segment control and communication systems control; a Data Receive, Record and Transmit System which receives all input image data and records it on high density tape for further processing; an MSS Image Processing System for reformatting, radiometric and geometric correction of MSS image data; and a TM Image Processing System for reformatting, radiometric and geometric correction and product generation of TM image data.

The Landsat D ground segment has been designed to process 200 MSS scenes per day (approximately 30 x 10^6 bytes/scene) that are reformatted and radiometrically corrected and have geometric correction data appended. This data is sent to EROS Data Center for further processing and product distribution. The ground segment will process 100 TM scenes per day that are reformatted and radiometrically corrected and have geometric correction data appended. An additional 50 TM scenes per day (approximately 300 x 10^6 bytes/scene) will be processed through geometric resampling with output products generated. The ground segment turnaround time will be less than 48 hours.

B. THEMATIC MAPPER GEOMETRIC CORRECTION OVERVIEW

The Thematic Mapper presents several unique problems for geometric correction which will be described in this paper. But first, we will present an overview of the geometric correction processing.

The driving system accuracy requirements are:

Radiometric Correction:	+1 quantum level relative within each band
Geodetic Registration :	0.5 pixel 90% of the time
Temporal Registration :	0.3 pixel 90% of the time

The purpose of geometric correction is to place image samples (pixels) of the ground scene at map grid locations so that (1) the geodetic location of image samples can be determined and (2) imagery from each satellite pass over a given area can be digitally registered.

To accomplish this purpose, the Landsat D System makes use of a World Reference System (WRS). The satellite orbit is precisely controlled and each orbit is repeated every 16 days (233 orbits). The WRS divides each of the 233 orbit paths into 248 scenes of 170 x 185 kilometers. A scene center is identified by a unique latitude and longitude and a fixed map grid system is defined for each scene.

Of course, image samples obtained by the TM will not fall on the WRS map grid system. During geometric correction, the TM data must be resampled onto the desired grid system.

Geometric correction is implemented as a two step process: Geometric Correction Data Generation followed by Resampling. The Correction Data Generation concept is shown in Figure 2. Information concerning time, spacecraft ephemeris (position and velocity), spacecraft attitude, scan mirror position, detector alignments, ground control points (for geodetic registration of the image), WRS scene identification and map projection are used to determine the location of each TM image sample on the map grid system. This location is called the map look-point. Correction Data defines a map look-point to map grid point transformation. In the Landsat D ground system, correction data is generated by first processing spacecraft attitude, spacecraft ephemeris and TM scan mirror position data. This information is used to generate an initial set of correction data called Systematic Correction Data. The Systematic Correction Data is then adjusted using ground control points to remove time, ephemeris, alignment and low frequency attitude errors.

Resampling is shown in Figure 3. Correction data is used to interpolate TM image samples and generate new samples at the map grid locations. Where possible, resampling is implemented by first performing a one-dimensional resampling pass along each detector line to generate hybrid pixels which are located along output map grid columns. The hybrid samples are then used in a one-dimensional vertical resampling pass to generate the sample located at the map grid intersection. The primary resampling technique is the four-point cubic convolution interpolation. This is a one-dimensional cubic spline interpolator[3] implemented by weighting the four surrounding pixels as shown in Figure 4. An assumption of equally spaced samples is made when using cubic convolution.

Discontinuities between forward and reverse scans of the TM have forced a modification of the resampling implementation. The geometric error mechanisms

creating this discontinuity will now be described.

C. TM SCAN GAP ERROR

The Landsat D temporal registration requirements translate to a requirement that the geometric error for a single TM scene (after correction) must be less than 3.2 meters (1 σ). This accuracy requirement coupled with the bi-directional scan mechanism have created a need to correct TM geometric errors that can be ignored in MSS processing. One such error which will be addressed in this paper is called scan gap. To explain scan gap, a brief description of the TM scanning is needed.

Each of the six TM high resolution spectral bands are imaged by sixteen detectors. These detectors are scanned in a direction approximately normal to the spacecraft ground track. The scan is bi-directional and produces an ideal ground pattern as shown in Figure 5. The broadening of the scan from its center to end is created by the increased slant range and is called the bow-tie effect.

An image line is created by sampling each detector every 9.611 microseconds as it is being swept along the ground by the scan mirror. The nominal active scan (duration of a forward or reverse scan) is 60.473 milliseconds with a 10.71 millisecond turnaround time. To create the scan pattern of Figure 5, the forward motion of the satellite (approximately 6.8 kilometers/sec) must be eliminated during the active scan. This is accomplished by a second scanning mirror (called the scan line corrector) which always scans back along the satellite ground track. The rate of the scan line corrector is 9.716 radians per second. This value produces the desired ground pattern for an orbit altitude of 712.5 kilometers and a ground velocity of 6.821 kilometers/sec. These are approximate mean conditions at 40 degrees north latitude. However, any combination of earth oblateness and periodic orbital variation will cause significant deviation from these design conditions. Along any output grid column, the line spacing within a scan will remain approximately equal, but it can be significantly different from the line spacing between two scans. The difference in line spacing, within a scan and between scans is called scan gap. That is, scan gap is zero when the spacings are equal, positive when there is underlap (missing data) and negative when there is overlap (extra data) between two scans. The Landsat D attitude will vary from 696 to 741 kilometers over the earth. Figure 6 shows the worst case range of scan gap due to altitude variation.

The scan gap size varies slowly across each scan due to the bow-tie effect, scan line corrector rate error and scan mirror profiles. Over small regions of the scan (say 128 pixels) the gap sizes can vary at a higher rate due to 0 - 125 Hz spacecraft angular deviations (jitter). To handle worst case conditions, the Landsat D ground processing has been designed to process scan gaps ranging from -3 to +2 pixels with a gap variation as large as one pixel over 128 samples.

D. SCAN GAP PROCESSING

There are neary 3×10^8 output pixels in a TM scene. The ground processing requirements translate to an average processing rate allocation of 750,000 pixels/second for resampling. Generation of every pixel requires at least 8 integer multiplies and 6 adds when using cubic convolution. To meet these high processing rates, dedicated hardware is used which implements an arithmetic pipeline processing procedure at high speeds. The output image is dynamically segmented, and each segment is independently generated using a subset of input samples. Segments are then reformatted for a line by line generation of the output image[4]. The size of an output segment is 128 columns by approximately 17 output lines.

The Landsat D ground segment will implement a three-pass resampling process to resample the gap region between two scans. The first pass is called x-resampling. It generates hybrid pixels aligned along output map grid columns by using cubic convolution resampling along input lines as previously illustrated in Figure 3.

Figure 7 shows the hybrid pixel locations for two sweeps after x-resampling. The generation of samples at map grid locations requires the use of four unevenly spaced hybrid pixels between lines 15 and 18. The resampling weights to be applied in this gap region are a function of two parameters: the distance between the grid point and scan line 16 and the gap size. Note that the line spacing within scan k and scan k+1 may be assumed equal.

When performing high speed resampling, it is necessary to use precomputed sets of four weights. This avoids the significant overhead of generating the weights during processing. For Landsat D, weight sets are calculated every 1/32 pixel. In order to reduce the number of weight sets and to simplify the processing, an intermediate resampling pass called sweep extension (or E-resampling) is used. Starting with the hybrid pixels from scans k and k+1, scan k is extended (lines 17E, 18E, etc) using a spline interpolation[1] along output columns as shown in Figure 7. This extension continues until output grid pixels can be generated using cubic convolution with the hybrid pixels of the extended scan k+1 alone. The extension pass requires weight sets which are a function of one parameter, the gap size, because the extension lines are spaced an integer number of line spacings below line 16.

The last resampling pass, called y-resampling, is

performed after sweep extension. The output grid pixels can be generated using cubic convolution along the output grid columns. The hybrid pixels from scan k and the extension pixels are used in this pass.

The gap region between scans k+1 and k+2 are similarly processed by extending scan k+1 and performing y-resampling starting from the point at which processing of scan k was terminated.

By appropriately defining weight sets, both positive and negative gaps can be accommodated using sweep extension. This approach degenerates into standard cubic convolution when the gap size is zero. The next section of this paper describes the radiometric effects of the resampling technique.

III. SIMULATION

A. SIMULATION OVERVIEW

The purpose of this simulation is to demonstrate the resampling algorithm performance given the geometrically uneven sampling of the Landsat D TM. In the earlier discussion of the Landsat D system, it was seen that deviation from ideal sampling occurs due to various factors. Some of these factors are the scanning mechanism, its interaction with the rotating earth, spacecraft altitude and jitter, alignment uncertainties, etc. Here, we will analyze the radiometric errors that occur as a result of the TM sampling geometry. These errors will be examined and characterized with respect to their sources. This analysis addresses high resolution bands using cubic convolution resampling (as opposed to the thermal band and nearest neighbor resampling).

The sources of error in the output image may be classified as:

1. Input sample position error.
2. Input sample intensity error.
3. Resampling algorithm error.

In this work, our primary interest is in examinig the error source c). Thus, the error sources a) and b) are made zero (actually the error source b) is not really zero because of the sampling method used - see Appendix A).

The simulation is comprised of two steps. The first step is the generation of the input data; which consists of the input sample positions and intensities. The second step is the output image generation, or resampling. For meaningful results, both the steps of the simulation must have functional fidelity to the real system within the bounds of the objectives of this work. Typical and worst case sampling geometry is tested by introducing the distortions using parameter variation during the sampling process. Since the sampling geometry is defined in the simulation, the sample positions are exactly known and therefore, error source a) is zero.

B. SAMPLING AND RESAMPLING

Sampling, here, is the process of generating a set of sample intensities and their corresponding positions from a given input image. The output of the sampling process is the input data for the resampling process. The sample positions reflect the sampling geometry and the intensities reflect the test image and the modulation transfer function (MTF) of the TM.

The sampling process is done in three parts. First, a test image is generated. This is the image that is actually on earth, and is also called the ground image. This is represented as a 256 x 256 image. Before sampling is performed, this image is passed through the TM optics and electronics, and is thus modified. This is described by the TM MTF (the MTF also includes the nonideal sampling process itself). The MTF[5] can be approximately represented as a two-dimensional sinc function in the Fourier domain. By setting the first zeros of the two-dimensional sinc function at 1/2 cycles per sample interval along both the directions, the MTF is completely specified except for the amplitude, which is set to 1.0 at the dc point. Such an MTF definition has the advantage that it can be simply implemented in the spatial domain. The one-dimensional case is shown in Figure 8. In two dimensions, the equivalent spatial domain function is a flat square shaped window with length of two sample intervals in each direction. Convolving the ground image with this function results in the MTF filtered image which is then sampled.

$$p(x_1, x_2) = g(x_1, x_2) \circledast w(x_1, x_2) \qquad (1)$$
$$= \int_{\tau_1} \int_{\tau_2} g(\tau_1, \tau_2)\, w(x_1 - \tau_1, x_2 - \tau_2)\, d\tau_1 d\tau_2$$

where

- g is the ground image
- w is the window function (spatial domain equivalent of the MTF)
- p is the MTF filtered image
- $\circledast$ is convolution

The output sampling interval is set at four units in both directions. This defines the spatial domain equivalent of the MTF as an 8 x 8 window. The equations, equivalent to Equation (1) but in digital form are;

$$p(i,j) = \frac{1}{64} \sum_{l=-3}^{4} \sum_{k=-3}^{4} g(i+k, j+l), \quad 1 \le i, j \le 256 \qquad (2)$$

Finally, we come to the sampling itself. This step

is important because it is here that all deviations from 'perfect' sampling are incorporated for a correct representation of the real sampling geometry. The following geometric considerations are incorporated:

1. The scan is skewed with respect to the output grid.
2. The scan is skewed with respect to another scan.
3. There are gaps between the scans.
4. The lines within a scan are parallel to each other.
5. The input sampling interval is not necessarily equal to the output grid size.
6. The along line sampling interval is not necessarily equal to the cross line sampling interval.
7. The along line sampling interval is not necessarily same from one scan to the next.
8. The cross line sampling interval is always constant.
9. The along line sampling interval is constant within a scan.

Various combinations of the above form typical or worst case sampling geometries. The geometries can be easily formed and tested with respect to the resampling radiometric fidelity.

The sampling method used (Appendix A) also introduces a radiometric error. This error occurs mostly at areas of changing intensity. It is a small error when smooth, edge free images are used, and may be considered as part of the radiometer nonlinearity and noise.

Resampling is performed on the sampled data (consisting of a set of sample intensities and positions). In essense, the resampling process is the estimation of intensities of the map grid points from the given input samples. As explained in Part II, the image is segmented, and each segment is processed independently using a three-pass resampling algorithm. A segment is defined as about 16 input lines by 32 output pixels in this simulation. Thus the image is divided into 8 segments; which allows for the analysis of segment boundary error.

For cubic convolution resampling, the cubic convolution alogrithm is used for interpolation in the x-resampling and y-resampling passes. This algorithm cannot be used for extension line generation (or E-resampling), however. This is because the samples used for interpolation are not evenly spaced as they are in the other two passes. A four-point cubic spline function has been used to perform the interpolation in E-resampling. This method was found to be the best of four tested - a) Linear 2-point, b) Inverse distance 4-point, c) 4-point polynomial (Lagrange) and d) Cubic spline 4-point. A modified cubic spline is used because the hardware for resampling limits interpolation weights to be of magnitude less than 1.0

C. RESULTS

In this section, test images will be defined, sampling geometries shown and the results of resampling displayed. A 256 x 256 image is used to represent a continuous image. The sampling interval is chosen to have a resolution about four times larger; thus producing 64 x 64 samples nominally. There are a number of reasons for doing this. Accuracy in assigning input sample values is preserved because the image is defined in a much finer grid. To see this, consider a smaller and smaller grid size (in comparison to the sampling interval) when, as a limiting case the image is continuous and the sample values are exact. There is a trade-off between greater accuracy of sampling and larger memory required for storing the image. In this case, a good balance was found in the parameters used. Finally, the MTF of the TM can be more accurately described over a larger number of points. An 8 x 8 window function does a better job of representing the MTF than say, a 4 x 4 or a 2 x 2 window would.

Two test images have been used. They are called 'Bulls Eye' and 'Checks' and are shown in Figures 9a) and 9b), respectively. The 'Bulls Eye' image was chosen because it has straight lines, curved lines and steps or edges; but is still simple enough structurally that any significant errors due to resampling can visually be detected. Starting with the innermost circle and proceeding outward, the intensity levels are 120, 180, 120 and 60. All intensity steps are 60 units. The reason for this is explained in Section D. The 'Checks' image was chosen to represent a portion of earth that has a lot of small fields on it. The two intensity levels are 40 and 200. The size of the squares in 'Checks' has been chosen here as 7 to 8 input sample intervals on each side. Thus, each square represents an area of earth of about 12.5 acres. Both the images in Figure 9 are 256 x 256 and are ground images. The corresponding 256 x 256 MTF filtered images are shown in Figures 10a) and 10b).

Resampling is done for three sampling geometries. We call them Case 1, Case 2 and Case 3. The sampling geometry parameters are described in Table 1. Case 1 is when the samples are positioned exactly at the output map grid points. This case does not require any resampling because the intensity at the output map grid points is exactly equal to the corresponding input sample value. However, it has been included here as a perfect case with which others may be compared.

In order to have a common base of comparison for all images, the 64 x 64 result of resampling is interpolated to 256 x 256 using the cubic convolution algorithm. The result of doing this on Case 1 is shown in Figures 11a) and 11b), respectively. These are called

base images - Base Bulls Eye and Base Checks. The results of resampling using Case 2 and Case 3 are shown in Figures 12 and 13, respectively. Case 2 represents a typical case of scan geometry distortion and Case 3 represents a worst-case situation.

D. ERROR ANALYSIS

From a visual inspection of the results of resampling there are a number of observations that can be made. From Figure 11, it can be seen that cubic convolution acts as an edge enhancer. Figures 11, 12 and 13 also show that image segmentation does not introduce any artificial intensity steps at segment boundaries. Large gaps between scans is the single biggest source of error in the resampling process. The algorithm tends to fill gap areas with a smooth variation in intensity, which is the best that can be done under the circumstances. Due to variation in the position of an intensity step in relation to a gap, certain structural information may be distorted. An example of this is the resampled result of Case 3 (Figure 13). Examining this result along with the scan geometry shows that the distortion occurs because of the gap between scan 1 and scan 2. Recall that we are dealing with the worst case situation here and that it rarely occurs. A more typical scan geometry distortion is Case 2 and examining Figure 12 we see that no distortion is visible.

The output image is a blown up version of a small portion of a real TM image. The latter is approximately 6500 x 6500 pixels, representing an area on earth of about 170 x 185 kilometers. The image dealt with in this paper is 64 x 64, and therefore, represents an area on earth of about 1.7 x 1.85 kilometers. This area is further blown up by a factor of four on each side so that a 256 x 256 pixel image now represents the same 1.7 x 1.85 kilometer area. This form of display is suited for this study because it shows a detailed and magnified view of the errors incurred.

Another method of evaluating the resampled images is also presented. It is called the percent error histogram. Geometric distortion and gross radiometric errors can be detected by visually comparing two images. Certain other kinds of errors are, however, hidden. Shifts in the image and smaller radiometric errors are an example. To detect image shifts, the two images must be registered. For detection of radiometric errors, the registered images must be evaluated at each pixel for differences in intensity. The percent error histogram does both of these tasks and provides valuable information for error characterization.

Specifically, the two images to be compared are differenced and the difference is expressed as a percentage of the magniture of the step size in the original ground image. It is clear, therefore, why all steps in the original image should be of the same magnitude for this error analysis to be consistent. Care has been taken to ensure this in both the 'Bulls Eye' and the 'Checks' images. A histogram of the difference image is then computed and this is called the percent error histogram.

The amount of error in a resampled image is reflected in the sharpness of the percent error histogram about the zero error point. Provided there are no systematic image intensity shifts, the histogram should be symmetric about the zero error point. Usually, the histogram also has its peak at this point (i.e., the single largest majority of pixels have zero error). The greater the spread about this point, the poorer we may expect the resampled image to be. Figures 14, 15 and 16 display the percent error histograms for both the 'Bulls Eye' and the 'Checks' image. Figure 14 shows the percent error histogram of the base image with respect to the MTF filtered image (Figure 11 with respect to Figure 10). Figures 15 and 16 show the percent error histograms respectively, of the resampled output image for Case 1 and Case 2 with respect to the base image (i.e., Figures 12 and 13 with respect to Figure 11).

It can be seen that for all cases tested, the histogram peaks occur at %error = 0. Error profiles are crudely symmetric about this point. We can conclude that:

1. Most of the image pixels come out of the resampling process without incurring any error at all.
2. There are no bias effects - no image intensity shifting due to resampling.

Figures 14, 15 and 16 also show that as the gaps and skews get larger, the related percent error histogram gets more spread out about the zero error point; which indicates that larger errors are encountered. Comparing Figures 14a), 15a) and 16a) with Figures 14b), 15b) and 16b) respectively, it is evident that the latter histograms have greater variances than the former. This is because the 'Checks' image has a greater step or edge footing than does the 'Bulls Eye' image.

Note that all histograms are displayed on a square root scale along the y-axis and a linear scale along the x-axis. This makes the smaller errors more visible in the histogram.

IV. ACKNOWLEDGMENTS

The authors gratefully acknowledge the contributions of members of the Systems Engineering Group at General Electric Space Systems in making this work possible.

V. REFERENCE

1. Hsieh S. Hou and Harry C. Andrews," Cubic Splines for Image Interpolation and Digital Filters," IEEE Trans. on Acoustics, Speech and Signal Processing, Vol. ASSP-26, No. 6, 508-517, Dec. 1978

2. Theodore C. Apeli and William Wolfe, "Landsat D, The Next Generation System," Western Electronic Show and Convention, Sept. 18-20, 1979

3. R. Bernstein, "Digital Image Processing of Earth Observation Sensor Data," IBM Journal of Res. and Dev., Jan. 1976

4. Jon E. Avery and James S. Hsieh, "Geometric Correction Resampling for the Landsat D Thematic Mapper," 1981 International Geoscience and Remote Sensing Symposium, Washington, D.C., June 8-10, 1981

5. Hughes Aircraft Company, "Thematic Mapper Detailed Design Review Package," Hughes No. D4596-SCG80201R, June, 1978

PARAMETER	CASE 1	CASE 2	CASE 3	PARAMETER	CASE 1	CASE 2	CASE 3
G_{1L}	0.0	1.57	3.0	AL1	4.00	4.24	4.24
G_{1R}	0.0	0.04	1.27	AL2	4.0	4.2	4.2
G_{2L}	0.0	0.26	0.73	AL3	4.00	4.24	4.24
G_{2R}	0.0	1.72	2.73	AL4	4.0	4.2	4.2
G_{3L}	0.0	1.32	2.3	CL	4.00	4.24	4.24
G_{3R}	0.0	0.78	0.9				

G_{IL} - LEFT GAP BETWEEN SCAN I AND SCAN I+1

G_{IR} - RIGHT GAP BETWEEN SCAN I AND SCAN I+1

ALI - ALONG LINE SAMPLING INTERNAL IN SCAN I

CL - CROSS LINE SAMPLING INTERNAL

Table 1. Definition of Cases

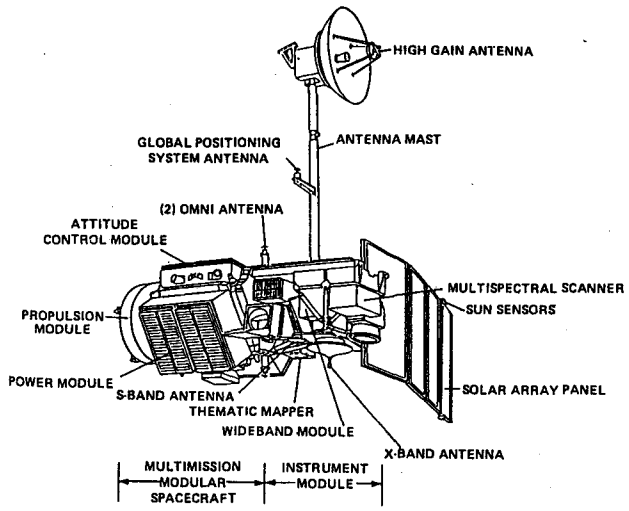

Figure 1. Landsat D Flight Segment

APPENDIX A: THE SAMPLING METHOD AND THE ERRORS IT INTRODUCES

Positions of the samples on the image are known once the sampling geometry is defined. The intensity assigned to the sample is the same as the intensity of the pixel within whose boundaries the sample falls. The error that such a sampling method introduces is analyzed here.

Assume that a step S occurs in the ground image. Due to the MTF, this step is diffused so that maximum variation of S/8 occurs from one pixel to the next. Using the sampling method described above, the sample intensity could be in error by $\pm$ (S/16). If we assume a uniform distribution of this error with mean zero, the standard deviation of this error is $S/8\sqrt{12}$.

In the two images used, the 1 σ step values are:

7.35 in the Bulls Eye image.
26.6 in the Checks image.

Thus, the respective 1 σ radiometric errors in sampling are, $7.35/8\sqrt{12}$ and $26.6/8\sqrt{12}$, which are:

0.265 1 σ radiometric error in Bulls Eye.
0.96 1 σ radiometric error in Checks.

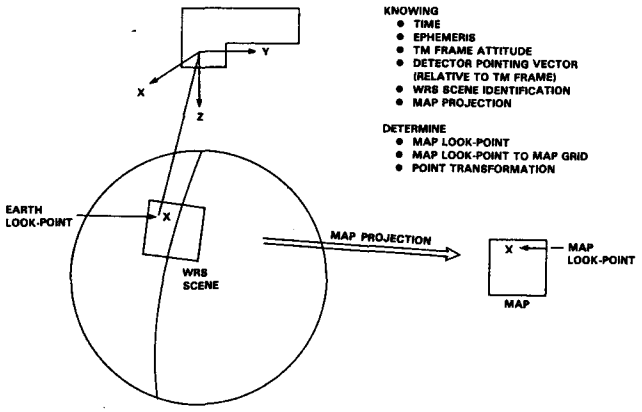

Figure 2. Correction Data Generation Concept

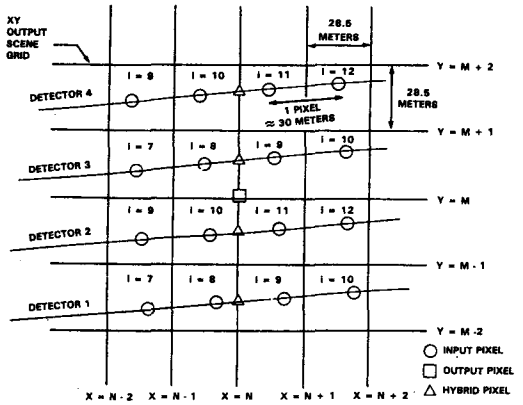

Figure 3. Location of Input Pixels on Output Grid

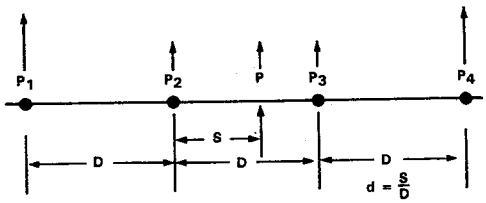

RESAMPLING CALCULATION

$$P = \sum_{I=1}^{4} P_I W_I$$

WHERE,

P_I ARE THE ON GROUND SAMPLES

P IS THE RESAMPLED VALUE

RESAMPLING WEIGHTS:

$W_1 = 4 - 8(1+d) + 5(1+d)^2 - (1+d)^3$

$W_2 = 1 - 2d^2 + d^3$

$W_3 = 1 - 2(1-d)^2 + (1-d)^3$

$W_4 = 4 - 8(2-d) + 5(2-d)^2 - (2-d)^3$

Figure 4. Cubic Convolution Resampling

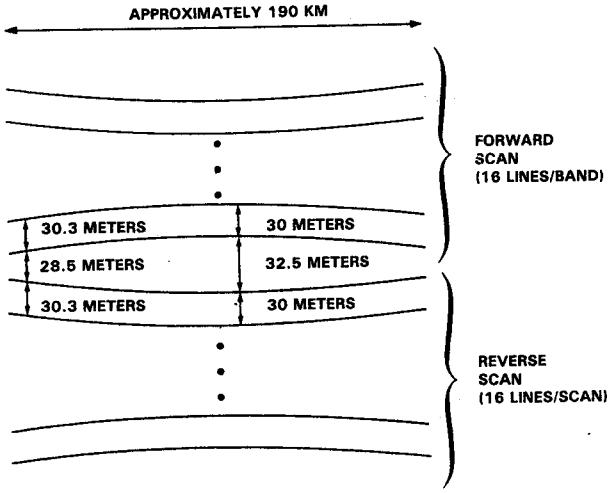

Figure 5. Ideal TM Scanning

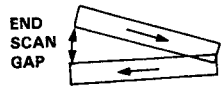

EARTH LOCATION	RANGE OF END SCAN GAP IN PIXELS*
NORTHERN HEMISPHERE	0.7 TO 0.8
45°N	0.4 TO 0.6
EQUATOR	0.2 TO 0.8
45°S	0.9 TO 0.1
SOUTHERN	1.6 TO 0.8

*INCLUDES SCAN WIDTH, SLC AND BOWTIE EFFECTS

Figure 6. Range of Scan Gap Due to Altitude Variation

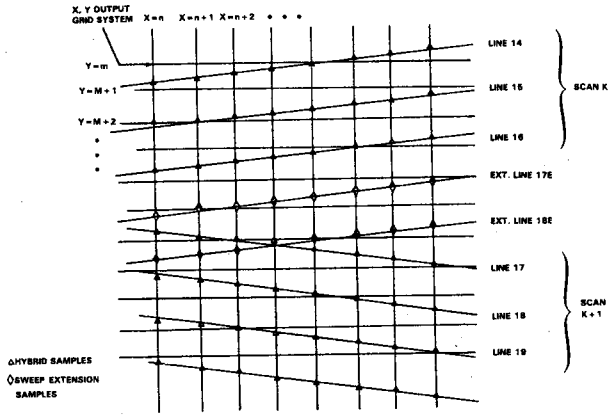

Figure 7. Scan Gap Processing With Sweep Extension

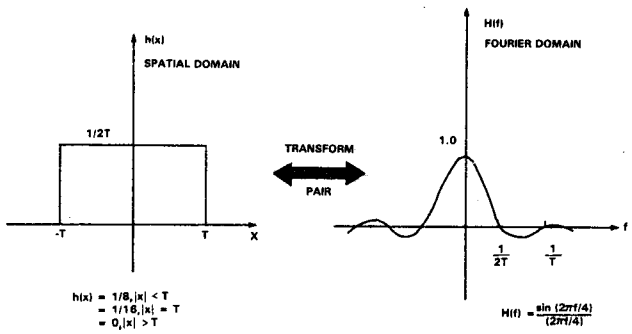

Figure 8. Inverse Fourier Transform of Sinc Function

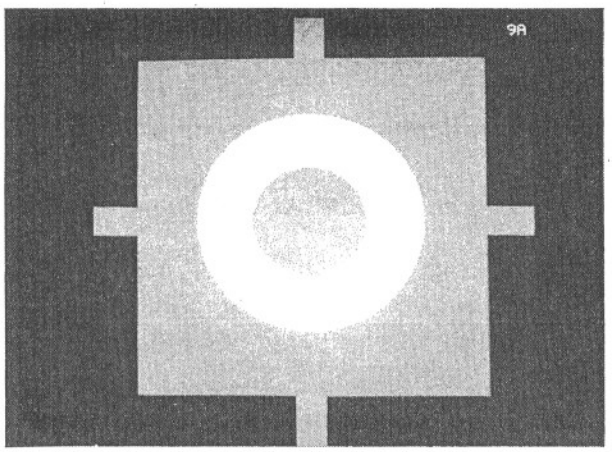

(a) Bulls Eye

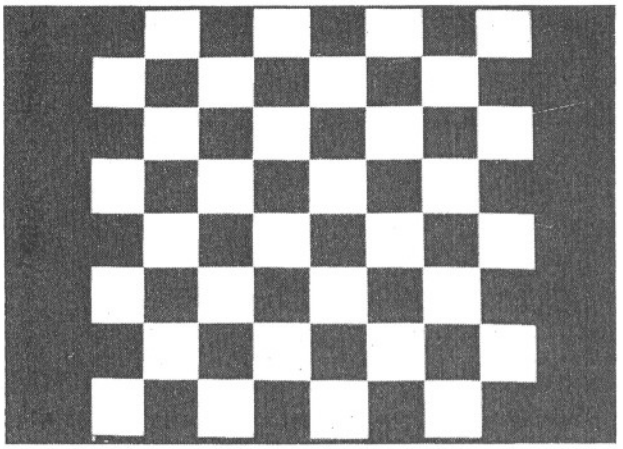

(b) Checks

Figure 9. Ground Images

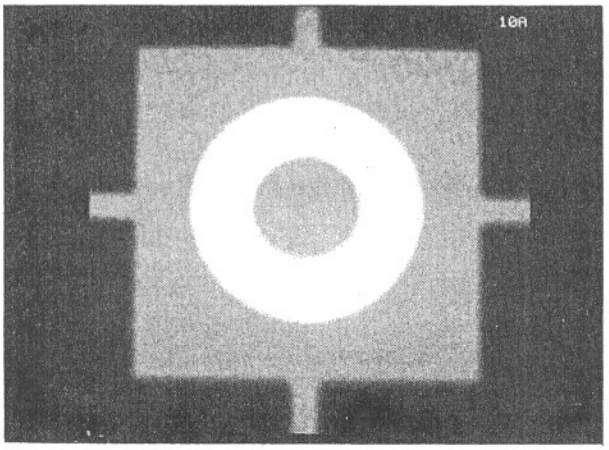

(a) Bulls Eye

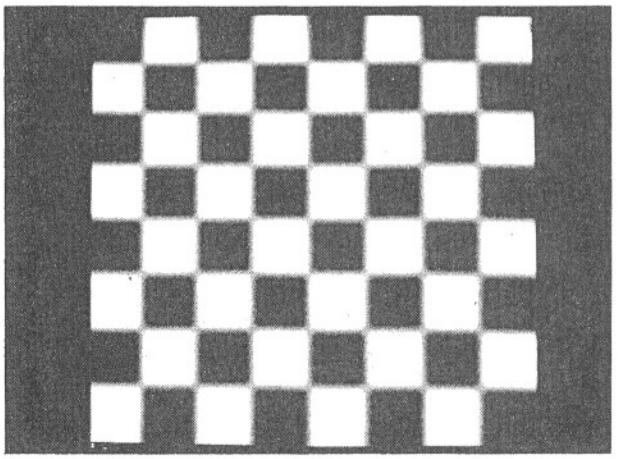

(b) Checks

Figure 10. MTF Filtered Images

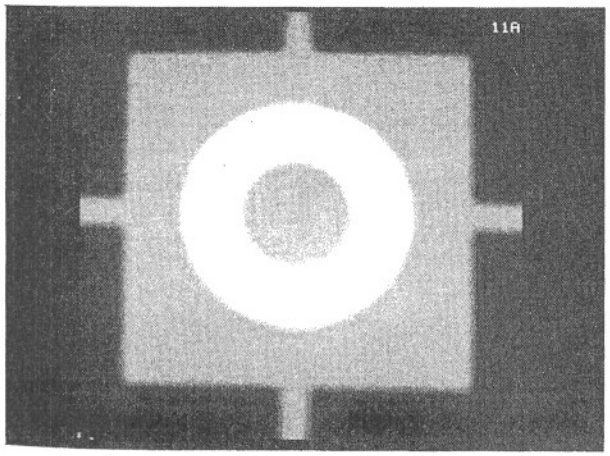

(a) Bulls Eye

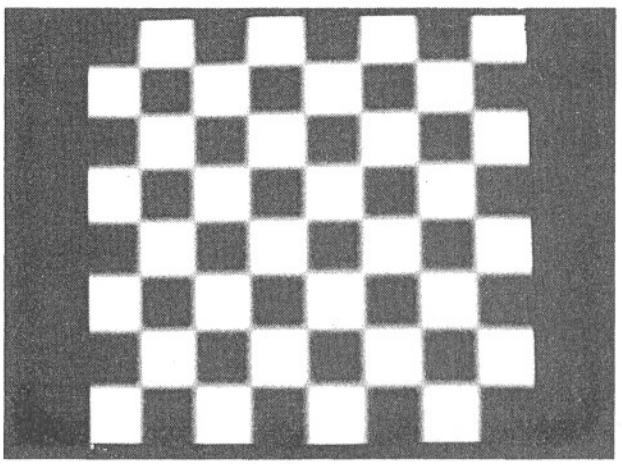

(b) Checks

Figure 11. Resampled Images, Case 1

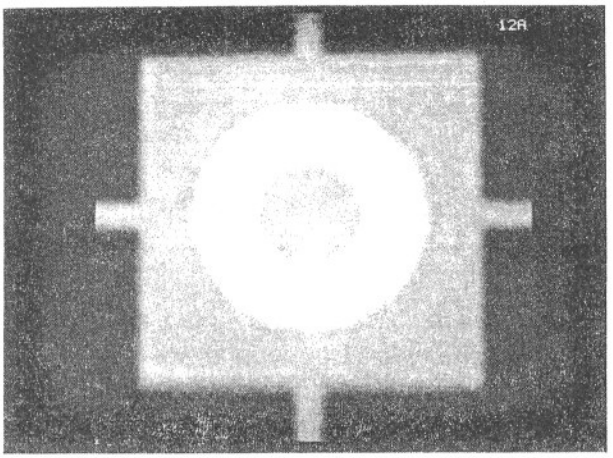

(a) Bulls Eye

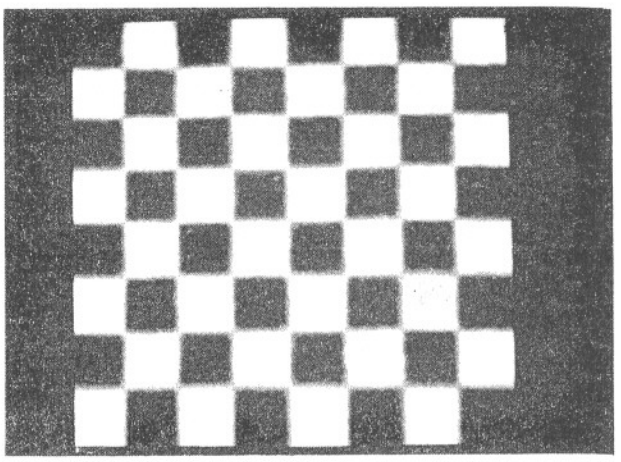

(b) Checks

Figure 12. Resampled Images, Case 2

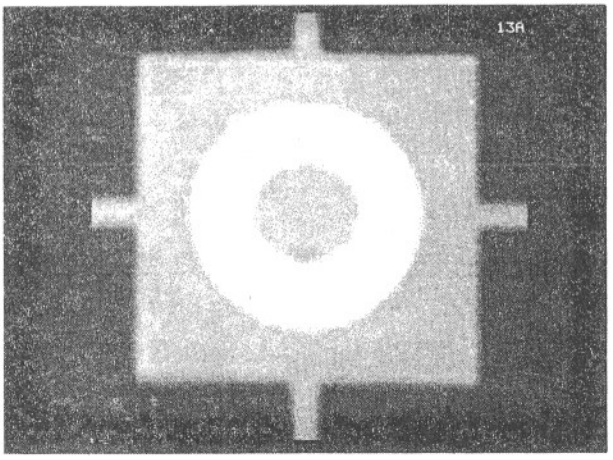

(a) Bulls Eye

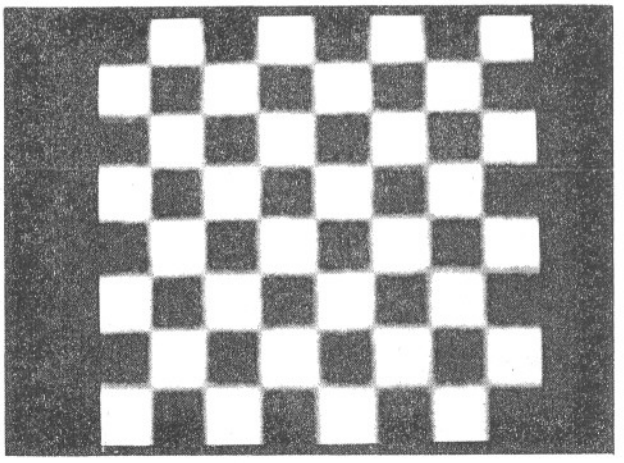

(b) Checks

Figure 13. Resampled Images, Case 3

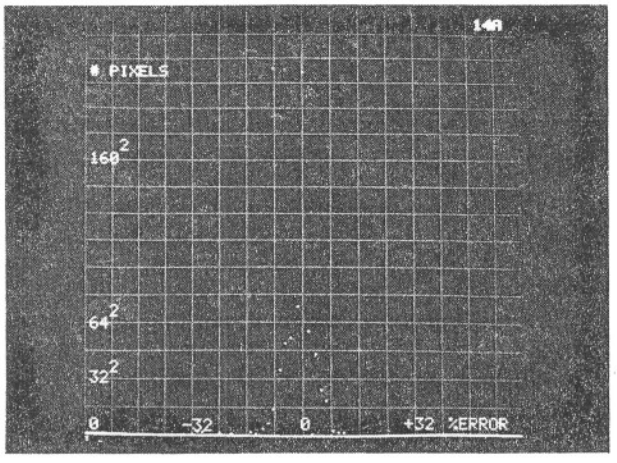

(a) Bulls Eye

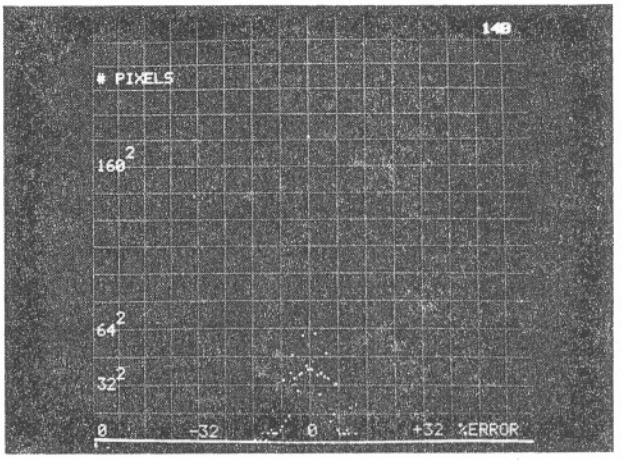

(b) Checks

Figure 14. Percent Error Histogram, Resampled Case 1 - MTF Filtered

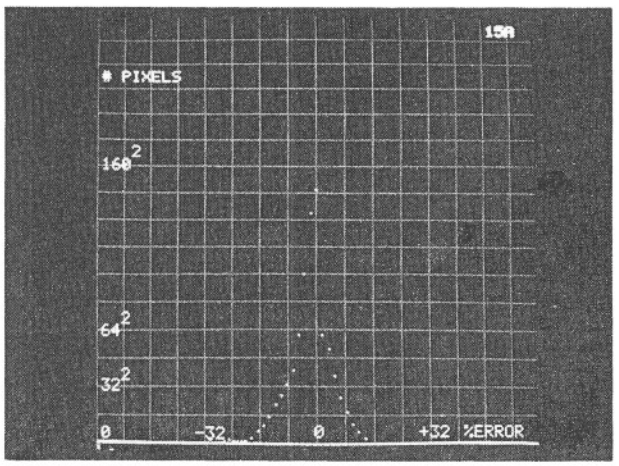

(a) Bulls Eye

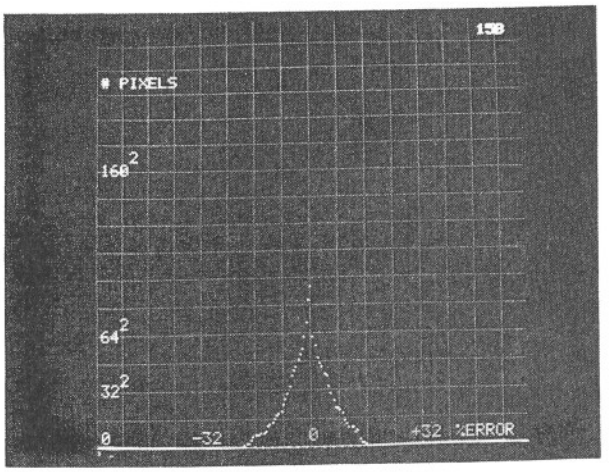

(b) Checks

Figure 15. Percent Error Histogram, Resampled Case 2 - Resampled Case 1

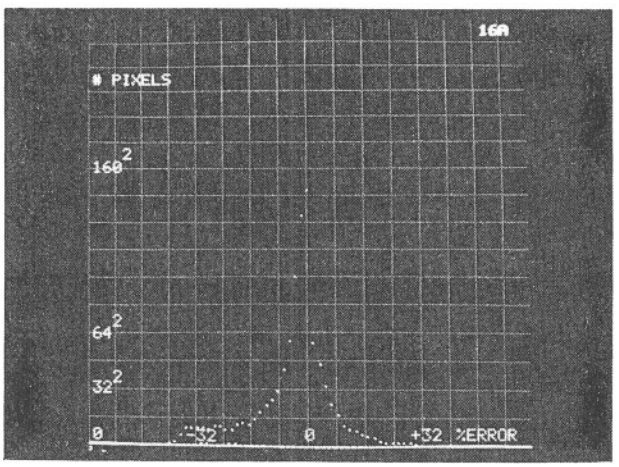

(a) Bulls Eye

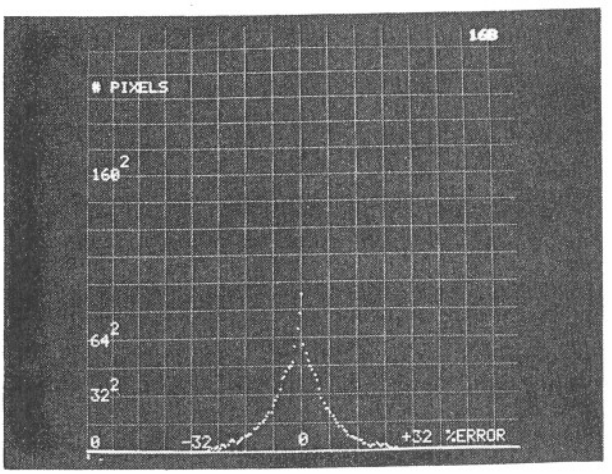

(b) Checks

Figure 16. Percent Error Histogram, Resampled Case 3 - Resampled Case 1

AUTHOR BIOGRAPHICAL DATA

Dr. Arun Prakash received his B.S. in Electrical Engineering from the Indian Institute of Technology, Bombay, India, in 1972. He received his M.S. and Ph.D. in Electrical and Computer Engineering from the University of Cincinnati in 1977 and 1979 respectively. His areas of interest are image processing, image reconstruction, signal processing and estimation. He joined General Electric in 1979 as a Systems Analyst and has worked on the design and analysis of the Landsat-D image processing system.

Eric P. Beyer, Landsat-D System Performance Engineer, joined General Electric in 1974 and has been active in signal processing; image processing algorithm development; and hardware/software implementations of processing algorithms. He has led the design effort for Thematic Mapper geometric correction, radiometric correction and automatic cloud cover assessment techniques. He received a B.S. in Electrical Engineering from Drexel University and a M.S. in Systems Engineering from the University of Pennsylvania.